We are IntechOpen, the world's leading publisher of Open Access books Built by scientists, for scientists

4,800
Open access books available

122,000
International authors and editors

135M
Downloads

Our authors are among the

154
Countries delivered to

TOP 1%
most cited scientists

12.2%
Contributors from top 500 universities

CLARIVATE ANALYTICS BOOK CITATION INDEX INDEXED

WEB OF SCIENCE™

Selection of our books indexed in the Book Citation Index in Web of Science™ Core Collection (BKCI)

Interested in publishing with us?
Contact book.department@intechopen.com

Numbers displayed above are based on latest data collected.
For more information visit www.intechopen.com

11

Multiscale Computer Aided Design of Microwave-Band P-I-N Photodetectors

Mikhail E. Belkin
Moscow State Technical University of Radio-Engineering, Electronics and Automation, Faculty of Electronics, Joint Research Laboratory "Microwave and Optoelectronic Devices", Moscow
Russian Federation

1. Introduction

Long wavelength InP-based p-i-n photodetectors (PD) are ubiquitous in modern optoelectronic circuits due to their inherent combination of ultra-high speed, high sensitivity in the most popular for modern telecom systems spectral range of 1.3-1.6 μm, and low bias voltages features that are impossible in principle for Si, GaAs or Ge counterparts. Typical material systems for the telecom spectral range are GaInAsP and GaInAs on InP substrate (Capasso et al., 1985). Now in the number of classical and present-day works (see, e.g. Bowers & Burrus, 1987; Beling & Campbell, 2009) is well-proved that compound semiconductor p-i-n photodetectors have the valid merits such as: high responsivity (up to 1 A/W), lowest dark current (below 10 fA), ultra-high bandwidth (up to 100 GHz and above), possibility of monolithic optoelectronic receiver module creation on common InP substrate.

Through a wide time period this type of PD found the most intensive application inside a receiver of the long-haul digital fiber-optic systems. But recently the p-i-n PDs for the wavelength of 1.3 and 1.55 μm are advancing in various RF and microwave photonic apparatus, particularly, in microwave-band optoelectronic oscillators (X.S.Yao, 2002), frequency converters (J. Yao, 2009), as well in so called photonic antennas for the base stations of radio over fiber (RoF) systems (Sauer et al., 2007). While designing a receiving module for the above devices and systems the stage of circuit schematic development referred to active and passive, electronic and photonic components' modeling would be most complicated and labour-intensive. Based on microwave IC design practice in this case the modeling is realized as a description of electrical and optical features of the integrated functional elements by means of mathematical equations, equivalent circuits or tables.

At present time computer-aided design (CAD) exploitation for innovative high-tech production R&D acceleration is a common way (Minixhofer, 2006). This is especially important for microwave semiconductor component base with measurement equipment and experimental work's cost being considerably more expensive compare to that in lower frequency bands. Using modern CAD software the next two approaches may be relevant for this case: by means of so-called physical models and by means of equivalent circuit models. A physical modeling is generally the most accurate but at the same time the most complicated. It is executed through a computer simulation of dedicated physical processes

running in the semiconductor chip's epitaxial layers. On the other hand, equivalent circuit model is simpler and includes current and voltage sources as well as passive elements that subject to frequency band are built on a linear circuitry with lumped (for RF band) or distributed (for microwave band) parameters. Correct simulation of the real device features is ensured by the account of nonlinearity and lag effects in the sources and passive elements. Their parameters and characteristics are specified by the DC or low-frequency measurements also by the small- or large-signal mode measurements in operating band and adjusted due to parametric optimization process. The main advantage of the approach is in clarity of device operation scripts and in versatility for the same class components when the parameter spread could be simply taken in account by proper changing the numerical value of the separate element. Therefore, a simulation issue optimal decision based on criteria of accuracy and computation time would rely on multiscale combination of the physical and equivalent circuit models. For computations the means of one or a number of CAD tools could be applied. Such approach might be called as multiscale or end-to-end design.

Generally a transparent way for microwave photonic devices' computer design lies in simulating with a help of so called optoelectronic CAD (OE-CAD) tool (Lowery, 1997). Nevertheless, our review of modern commercial OE-CAD software has shown up their lack of development to simulate a microwave circuitry. An alternative approach is to model by two classes of CAD tools: so-called technology CAD or TCAD software (Blakey, 2008) and microwave-band electronic CAD or MW-ECAD software (Kielmeyer, 2008). By means of the first one a designer could realize the analysis procedures for a number of semiconductor chip physical, electrical and optical features and its DC characteristics; also simulate semiconductor laser, photodiode, transistor, or diode structure's small-signal frequency response. But for designing a number of relevant microwave photonics devices, e. g. optically controlled microwave amplifiers and switches, optoelectronic oscillators, transmitter and receiver optoelectronic modules, and so on one needs to know quite a number of the active semiconductor device parameters specifying its functioning in the operating bandwidth and in large-signal mode: output intercept point, harmonic and intermodulation distortions, large-signal output reflection coefficient. It is impossible to simulate the above features by the means of a TCAD tool. One more significant drawback of the tool is that the account of device package and assembling parasitic elements impacts is also impractical. This matter results in the solution error up to 30% even at the lower part of the microwave band that is growing along with a modulation frequency is being increased (Belkin & Dzichkovski, 2009).

The both issues are overcome by the application of ECAD tool optimizing for microwave band operation. The MW-ECAD tool special preference is in powerful electromagnetic (3D) analysis and optimization resources of microwave electronic circuitry and layouts design, for instance low-noise and power amplifiers, highly complex receiver optoelectronic modules. So introducing a convenient interface between these CAD tools one could realize multiscale end-to-end design of the device or module with microwave bandwidth. Usually for this goal well-known HSPICE interface is feasible. In this case, input data are multilayer semiconductor heterostructure with the certain cross section, and output data are a whole number of the outer parameters that totally and correctly characterize its features in microwave band. Also it might be a layout drawing of the module in development.

Thus, there exists a need for a reliable circuit-level photodetector model suitable for a designer of receiving modules of modern optical fiber-based systems and microwave photonics devices. In this chapter our recent results of the combined TCAD&ECAD and

solitary MW-ECAD simulations for designing a long wavelength microwave-band p-i-n photodetector as a basic component of a multichannel analog system are presented.

2. General review

Generically, a photodiode as any electronic diode is a nonlinear device with a saturation effect and when it works in large-signal mode the fundamental signal is usually accompanied by a remarkable level of nonlinear distortions (Yu & Wu, 2002). The main distortion sources of the PD's conversion characteristic include absorption saturation, transit-time effects, and electric field screening arising from the space charge in the depletion layer (Williams et al., 1996). The latter effect also arises due to series resistance outside a junction region of a PD.

Nevertheless, in digital optical fiber systems handling with typical receiving power levels lower than 1 mW a photodiode is able to represent as linear device. On the other hand, in order to secure the needed spurious free dynamic range (SFDR) in the above microwave photonics devices and RoF systems the power levels may be up to 100 mW. For example a simple analysis of an opto-electronic oscillator model using quasi-linear interpretation results in the next expression for self-oscillating regime (X.S.Yao, 2002):

$$I_{ph}R \geq \frac{V_\pi}{\pi}, \tag{1}$$

where I_{ph} is the PD photocurrent; R is the PD load impedance; V_π is so called half-wave voltage of Mach-Zehnder modulator. Relationship between the photocurrent I_{ph} and the PD optical power P_0 is addressed to the well-known formula:

$$I_{ph} = P_0 S_0 \ , \tag{2}$$

where S_0 is the PD current responsivity. From (1) and (2) one can clearly conclude that self-oscillating condition could be simplified through increasing optical power at PD input. Namely, for typical values of R=50 Ω, V_π=5 V, S_0=0.5 A/W it would be more than 64 mW. Naturally, it is unpractical to represent photodiode in such a regime as a linear element.

Large-signal operation of PD in the above-mentioned devices and system called out an additional issue that a pre-amplifier following the PD must concurrently have low noise figure and enough high linearity. A good chance to circumvent this issue is in utilizing a special type high-linear PD and a scheme without pre-amplifier (Joshi & Datta, 2009). Note that operating the photodiodes at larger photocurrent has added benefit of reducing overall noise figure of the device or link. But an employment of special type PDs that are structurally more complicate than standard ones might degrade the economical features of optical receivers. Thus, a direct linearity comparison of the widespread top-illuminated PD and middle-power microwave transistor amplifier is a subject of practical interest.

As known from RF and microwave amplifier design experience (Kenington, 2000), device linearity in large-signal mode is regularly characterized by so-called harmonic and inter-modulation distortions (IMD). Among them a two-tone third-order IMD (IMD3) is the most severe issue in design practice. The reason is in their closer positioning to carrier signals to allow rejecting by filters. Also for super wideband microwave photonic devices and systems when the bandwidth is more than an octave the two-tone second-order IMD (IMD2) is in

great importance too. Generally, two-tone IMD is a product of passing two unmodulated carriers at the frequencies of f_1 and f_2 through a nonlinear device. When viewed in the frequency domain, output spectrum of the circuit includes besides f_1 and f_2 a lot of overtones. In the general case of distortions created by any order nonlinear circuit new frequencies will be generated in the form:

$$f_i = mf_1 \pm nf_2 \tag{3}$$

where m and n are positive integers (including zero), m+n is equal to the order of the distortion. Then in the case of second-order nonlinearity each of the two tones will have a second harmonic and additional sum and difference beatings will occur at frequencies of $f_1 \pm f_2$. Also in the case of third-order nonlinearity each of the two tones will have a third harmonic and additional sum and difference beatings will occur at frequencies of $2f_1 \pm f_2$ and $2f_2 \pm f_1$. These overtones are known as second-order and third-order intermodulation products correspondingly. One can calculate the above distortions through carrier transport equations (Williams et al., 1996) but the most simple and accurate way lies in measuring them in microwave band.

An obvious methodological drawback of IMD is referred to the dependence from powers of input signals that make impossible to compare devices at different input powers. To cope with it another well-known figure of merit for microwave amplifier linearity so called output intercept point (OIP) (Kenington, 2000) is widespread for microwave-band optoelectronic devices acting in large-signal mode. Following RF and microwave amplifiers, a rough estimate of the photodiode's 2-order OIP (OIP2) and the 3-order OIP (OIP3) can be produced by the following simple equations.

$$OIP2 = P_{out} - IMD2\,, \tag{4}$$

$$OIP3 = P_{out} - IMD3/2\,, \tag{5}$$

where P_{out} is output AC power of the fundamental tone in the photodiode load. Each parameter is usually expressed as a power in dBm. However, a common practice to define

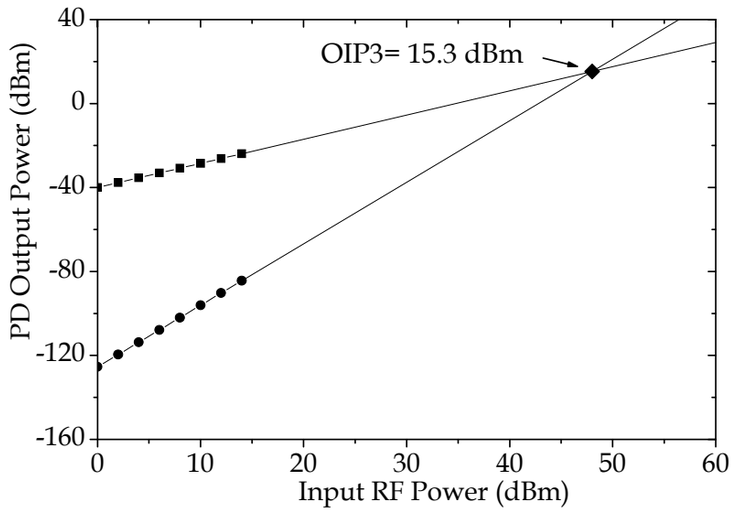

Fig. 1. A typical example of OIP3 determination for a photodiode

No	Description of the PD under test	Small-signal bandwidth	Output Intercept Point	Reference
1	Large optical cavity p-i-n waveguide InGaAs photodiode	20 GHz	OIP3 (-9 V, 1 GHz)=15.3 dBm OIP3 (-9 V, 18 GHz)=2.4 dBm	Jiang et al., 2000
2	Uni-traveling carrier waveguide integrated InGaAs photodiode	20 GHz	OIP3 (-5 V, 1 GHz)=24 dBm OIP3 (-5 V, 18 GHz)=8 dBm	Liao et al., 2003
3	Backside illuminated uni-traveling carrier InGaAs photodiode	10 GHz	OIP3 (-3 V, 10 GHz)=32 dBm OIP3 (-5 V, 10 GHz)=40 dBm	Gustavsson et al., 2005
4	GRIN lens-coupled top-illuminated InGaAs photodiode	6.5 GHz	OIP3 (-5 V, 0.83 GHz)=43 dBm OIP3 (-9 V, 0.83 GHz)=49 dBm	Joshi et al., 2008
5	P-i-n waveguide InGaAs photodiode	20 GHz	OIP3 (-4 V, 1.1 GHz)=32.6 dBm	Draa et al., 2008
6	Charge compensated modified uni-traveling carrier InGaAs photodiode	23 GHz	OIP3 (-7 V, 0.31 GHz)=52 dBm	Beling et al., 2008
7	Partially-depleted absorber back-illuminated mesa structured photodiode	10 GHz	OIP3 (-1 V, 1 GHz)=30 dBm OIP3 (-3 V, 1 GHz)=38 dBm OIP3 (-5 V, 1 GHz)=43 dBm	Tulchinsky et al., 2008
8	Top-illuminated InGaAs p-i-n photodiode	8 GHz	OIP3 (-2 V, 1 GHz)=17 dBm OIP3 (-8 V, 1 GHz)=30 dBm OIP2 (-2 V, 1 GHz)=33 dBm OIP2 (-8 V, 1 GHz)=46 dBm	Godinez et al., 2008
9	Top-illuminated InGaAs planar p-i-n photodiode	3.2 GHz	OIP3 (-16 V, 0.83 GHz)=49 dBm	Joshi & Datta, 2009
10	Ge n-i-p on silicon-on-insulator substrate photodiode	4.5 GHz	OIP3 (-5 V, 1 GHz)=20 dBm OIP2 (-5 V, 1 GHz)=40 dBm	Ramaswamy et al., 2009
11	Backside illuminated InGaAs p-i-n photodiode array	8 GHz	OIP3 (-2 V, 5 GHz)=32.5 dBm	Itakura et al., 2010
12	Modified uni-traveling carrier InGaAs photodiode with cliff layer	24 GHz	OIP3 (-5 V, 0.32 GHz)=45 dBm OIP3 (-9 V, 0.32 GHz)=50 dBm	Li et al., 2010

Table 1. Results of photodetector's output intercept point measurements

OIP relies on a graphical representation of measured amplitude curves for fundamental and second- or third-order IMD tones. Following it Figure 1 illustrates a typical example of OIP3 determination for a photodiode (Jiang et al., 2000) extrapolated from the measured data of fundamental (squares) and IMD3 (circles) plots. In the Figure's logarithmic scale on the both axes the graphs represent straight lines where the fundamental tone has a slope of 1:1 and IMD3 tone has a slope of 1:3.

Up-to-date there is a series of papers referred to OIP measurements. Table 1 lists the results of some of them.

At a glance the values of photodiode OIP were eventually increased and for today the highest OIP of more than 50 dBm possesses charge-compensated modified uni-traveling carrier InGaAs photodiode (Beling et al., 2008). Standard vertical-illuminated p-i-n PDs have some lower OIP values up to 46-49 dBm. The general tendencies for all types of PDs consist in decreasing OIP as the test frequency and the negative voltage bias are increased.

Another known property of nonlinear circuits is that vector addition of the output fundamental and harmonic components also determines a phase variation of the resultant output signal when the input level varies. This effect is a requisite of dynamic systems and as the figure of merit for microwave amplifier linearity is called amplitude-to-phase (AM-to-PM) conversion for single-tone mode that is usually expressed as a certain phase deviation, in degrees or radians at predetermined input power (Pedro & Carvalho, 2003). In the case of photodetectors the similar parameter in terms of power-to-phase conversion (PPC) is being investigate by a joint research team (Tailor et al., 2011) for emerging microwave photonics-based timing applications in the fields where it is important to precisely know the arrival time of light pulse such as RoF, phased-array radars, optical fiber coherent communications and so on. Our results of MW-ECAD's photodiode nonlinear modeling will be highlighted in section 4.

3. Combined TCAD&ECAD simulation

To illustrate effectiveness of multiscale approach, the end-to-end design of the photodiode modules with bandwidth near thirty gigahertz was fulfilled. At the first step following the modern CAD tools capabilities (see the Introduction), the simulation of the super high-speed pin-photodiode was carried out with the aid of Synopsys Sentaurus TCAD software tool[1]. Sentaurus package allows for correct modeling of the wide spectrum of semiconductor devices due to transport equations and various physical models combining. There is fundamental capacity of photodetector simulation too but up to date the examples of it are not frequently (see e. g. Zakhleniuk, 2007).

3.1 P-i-n photodiode heterostructure TCAD simulation

For the simulation a widespread mesa-construction with semi-insulator-buried and vertically-illuminated p-i-n photodiode heterostructure similar to partially-depleted absorber type (Tulchinsky et al., 2008) was selected (Figure 2). In the Figure: region 1 is p^+-type contact layer, region 2 – p-type buffer layer, region 3 – i-type absorption layer, region 4

[1] http://synopsys.com/home

- n-type buffer layer, region 5 – n^+-type contact layer. The mesa's material composition, layers initial doping levels and thickness selected for simulation are: region 1 - $Ga_{0.47}In_{0.53}As$, $5 \cdot 10^{18}$ cm^{-3}, 0.5 μm; region 2 –InP, $3 \cdot 10^{17}$ cm^{-3}, 3 μm; region 3 - $Ga_{0.47}In_{0.53}As$, $3 \cdot 10^{16}$ cm^{-3}, 1 μm; region 4 – InP, $3 \cdot 10^{18}$ cm^{-3}, 0.3 μm; region 5 - InP, $8 \cdot 10^{18}$ cm^{-3}, 2 μm. The substrate's doping level and thickness are $2 \cdot 10^{18}$ cm^{-3} and 300 μm correspondingly. The chip dimensions are 200x200 $μm^2$, the mesa's top diameter is 50 μm.

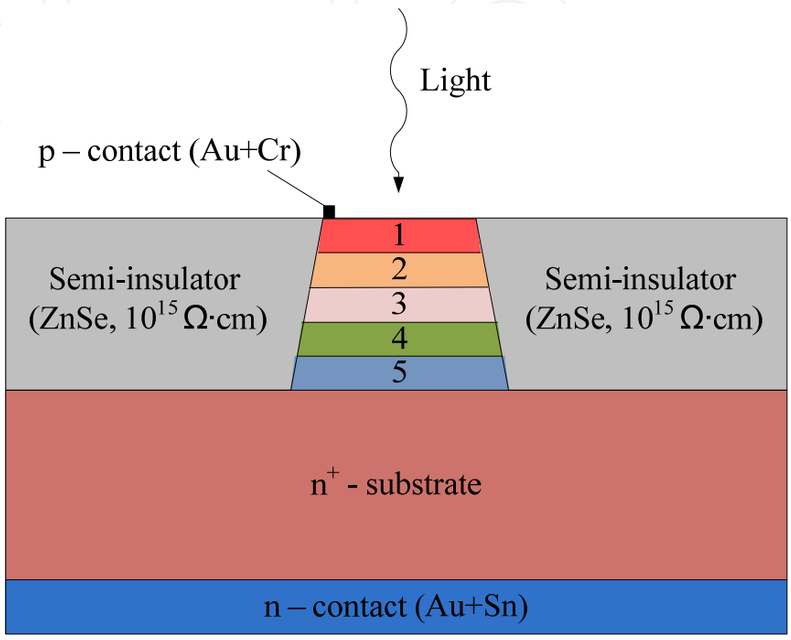

Fig. 2. The cross section of the photodetector in research

Such double-heterojunction p-i-n photodiode structure as will be shown below is lightly slower than more popular single-heterojunction one (Bowers & Burrus, 1987) but has a number of physics and technological advantages with minor deterioration of operating speed (Belkin et al., 2008):

- the possibility of the buffer and absorption layers precise doping;
- decrease of growth defects (growth pits, packing defects, absorption layer surface erosion);
- volatile components (such as As and P, and Zn doping agent) evaporation exclusion;
- the possibility of using InP "wide-gap window" effect that permits to collect photons on absorption layer without their surface recombination in the air-absorption layer interface;
- the possibility of desired form photodiode mesa-structure creation, using indium phosphide and solid solution etching selectivity, and small-area photodiodes forming selectivity;
- the possibility of compensating in part space-charge effect due to different thickness of the layers 2 and 4.

All the advantages above allow minimizing photodiode dark current ensuring maximum current responsivity.

The SYNOPSYS Sentaurus TCAD platform was used to model the Fig. 2's photodiode structure. The simulating procedure based on the following methodology. As the first step optical field distribution profile was inspected (Figure 3). In the result we determined that optical field is absorbed completely in the depletion layer 3 of Fig. 2 (dark horizontal stripe in Fig. 3). Then, by optical power-dependence reverse current-voltage characteristics computation we found that optimal photodiode operating voltage was -10 V (Belkin et al., 2008). The final step was AC small-signal current responsivity-frequency characteristics analysis and optimization in dependence of the absorption layer doping density, N_D, thickness, s and the photosensitive window width, w (in 2D-model).

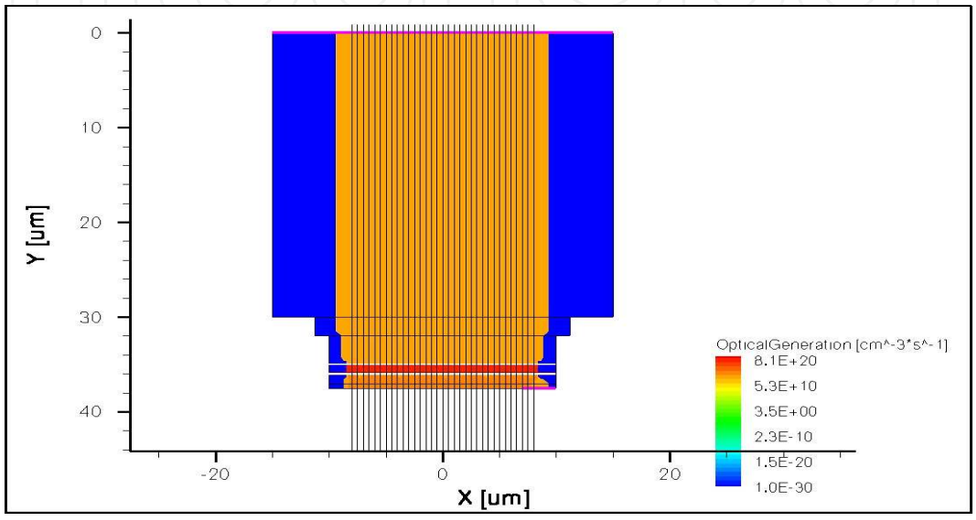

Fig. 3. Optical field distribution profile (The PD structure is upside-down to that of Fig. 2)

As known (Bowers & Burrus, 1987), the general limitations on the speed of p-i-n photodetectors are: 1) carrier drift time across depletion layer, 2) diode inherent capacitance charge/discharge time, 3) charge trapping at heterojunctions, 4) diffusing time out of undepleted regions, 5) package parasitic effects. Among them, in photodetector heterostructure with target bandwidth of 30 GHz the major effect is due to the first two factors because the hole trapping time even for abrupt p-InP/i-GaInAs heterojunction was estimated to be about 5 ps (Wey et al., 1995).

In the course of simulations by means of the program developed, some data for technology research and photodiode structure design, that are optimized for all the three above parameters, are received. First, optimal absorption layer doping density with s=1 μm and w=25 μm was investigated (Figure 4). Absorption region doping level analysis showed: 1) photodiode bandwidth was increased with the level diminishing, 2) there was no sense to provide lower than $N_D = 10^{16}$ cm^{-3} as the bandwidth became almost invariable (The latter is important from the technology point), 3) to meet the above project goal of 30 GHz the simply realized by well-known liquid-phase epitaxy $N_D = 1 \cdot 10^{-16}$ cm^{-3} is quite enough. That's why the above value was used in the future simulations.

Furthermore, optimal absorption layer thickness with $N_D = 1 \cdot 10^{-16}$ cm^{-3} and w=25 μm was investigated (Figure 5). Absorption layer thickness analysis showed: 1) as for super high-speed p-i-n photodiode it is necessary not to diminish, according to known results (see e.g.

Agethen, et al., 2002), but to increase the thickness for bandwidth enhancement because of the need to consider not only time of carrier drift through depletion region, but diode's self-capacitance charge/discharge time too; 2) optimal thickness of absorption region for photodiode modeled is near s=1 μm as for the larger ones the bandwidth became almost invariable. That's why the above value was determined as optimal for the project goal achievement.

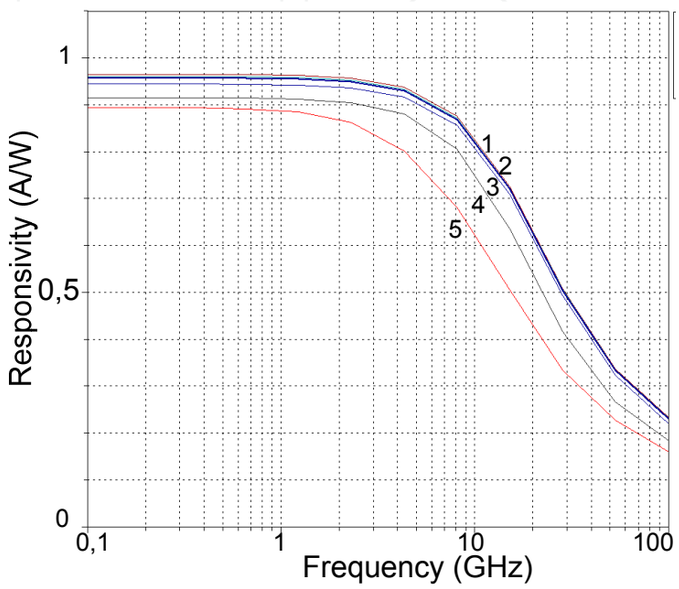

Fig. 4. The bandwidth vs. absorption region doping density simulation (1: N_D=8 ·10^{15} cm^{-3}; 2: N_D=1 ·10^{16} cm^{-3}; 3: N_D=2 ·10^{16} cm^{-3}; 4: N_D=3 ·10^{16} cm^{-3}; 5: N_D=4 ·10^{16} cm^{-3})

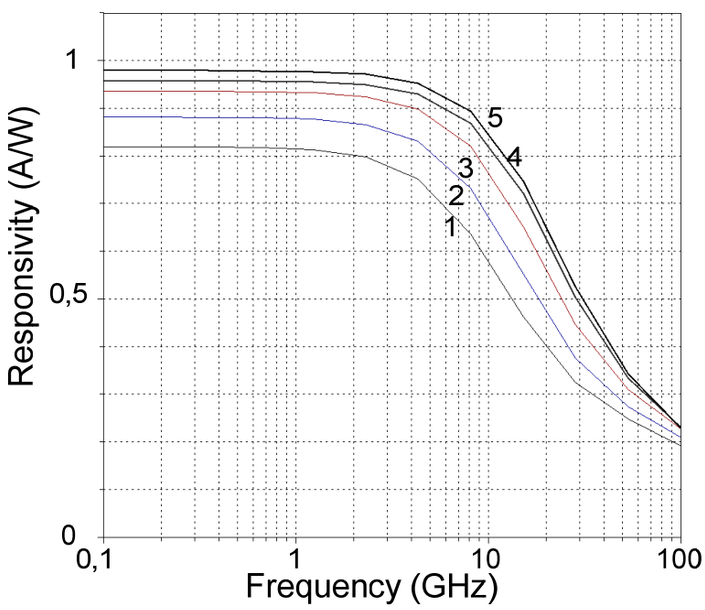

Fig. 5. The bandwidth vs. absorption region thickness simulation (1: s=0.3 μm; 2: s=0.55 μm; 3: s=0.8 μm; 4: s=1 μm; 5: s=1.3 μm)

Finally, the optimal photosensitive window width with $N_D=1\cdot10^{-16}$ cm^{-3} and s=1 μm was investigated (Figure 6). Photosensitive window width analysis showed: 1) the photodiode bandwidth was increased with the width diminishing; 2) the project goal value of 30 GHz is arrived when w≤22 μm that relatively similar with the other results (Bowers & Burrus, 1987; Agethen, et al., 2002).

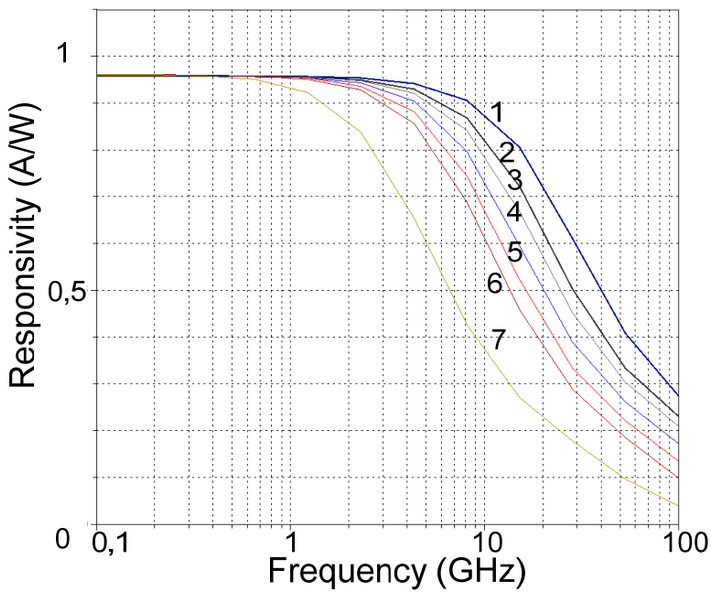

Fig. 6. The bandwidth vs. photosensitive window width simulation (1: w=18 μm; 2: w=20 μm; 3: w=22 μm; 4: w=24 μm; 5: w=26 μm; 6: w=28 μm; 7: w=30 μm)

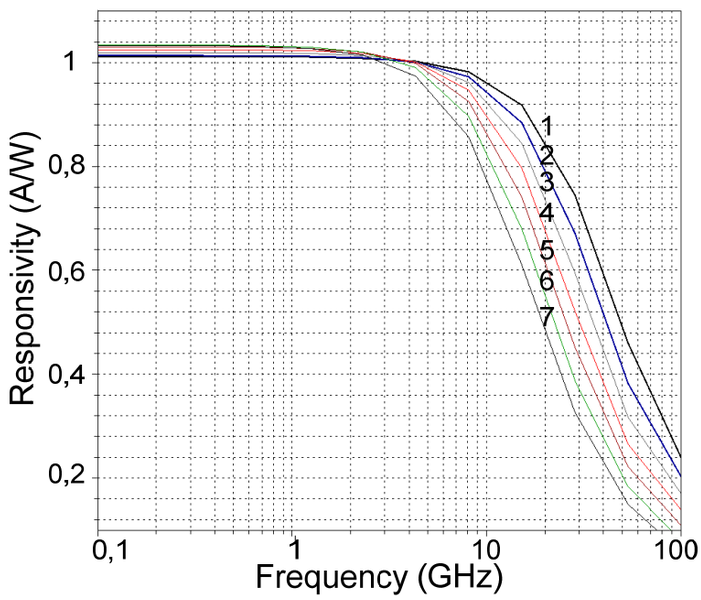

Fig. 7. The bandwidth vs. photosensitive window width simulation for a usual top-illuminated p-i-n photodiode structure with single heterojunction (1: w=18 μm; 2: w=20 μm; 3: w=22 μm; 4: w=24 μm; 5: w=26 μm; 6: w=28 μm; 7: w=30 μm)

Our last TCAD modeling was referred to the photodetector bandwidth estimation due to additional epitaxial layer introduction (Fig. 2, region 2). For this purpose the same photodiode structure response with closed region 2 was simulated (Figure 7). From the Figure one may conclude that the photosensitive window width needed for the project goal of near 30 GHz was increased slightly (up to 24 μm). So its effect has not to simplify substantively the mesa etching process.

3.2 P-i-n photodiode MW-ECAD simulation

As mention above for end-to-end design of a microwave-bandwidth photodiode an appropriate ECAD tool is required. The most convenient way for this microwave network research is the approximation by a physical equivalent circuit (Figure 8). In the Figure, I_{ph} is the complex photocurrent source (frequency F dependent), R_d, C_d, R_s are the p-i-n photodiode heterostructure differential resistance, intrinsic capacitance and serial resistance respectively. Furthermore, L_w and C_c are the connecting wire inductance and case capacitance approximation.

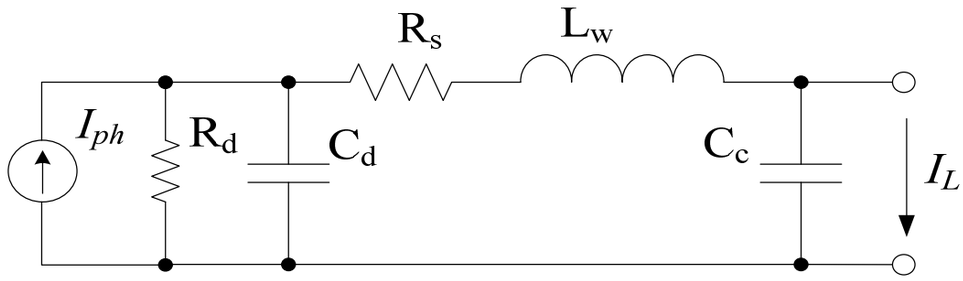

Fig. 8. The p-i-n photodiode electrical equivalent circuit

Based on the usual RF circuit simulation technique the photodiode transducer gain k_{pd} can be determined from this scheme as:

$$k_{pd} = I_L / I_{ph} \tag{6}$$

where I_L is complex load current. Then from the Figure 8:

$$\dot{k}_{ph} = \frac{(1 + j\omega C_c z_L)^{-1}(1 + j\omega\tau)}{1 - \omega^2 L_w C_d + j\omega C_d R_s + z_L(1 + j\omega C_d z_L)^{-1}} \tag{7}$$

where $\omega=2\pi F$, z_L is load impedance, τ is transit time.

The values of $I_{ph}(F)$, τ, R_d=3.5 MΩ, C_d=80 fF, R_s=21 Ω were found analytically from the Sentaurus program. Also the values of L_w and C_c=0.11 pF were determined experimentally by the microwave vector network analyzer. Figure 9 illustrates some results of the AWRDE [2] ECAD environment simulation. It follows from the graphs that the designer can realized twofold expansion of the photodiode 3 dB bandwidth (20 to 40 GHz) owing to the appropriate fitting of the connecting wire inductance L_w.

[2] http://web.awrcorp.com

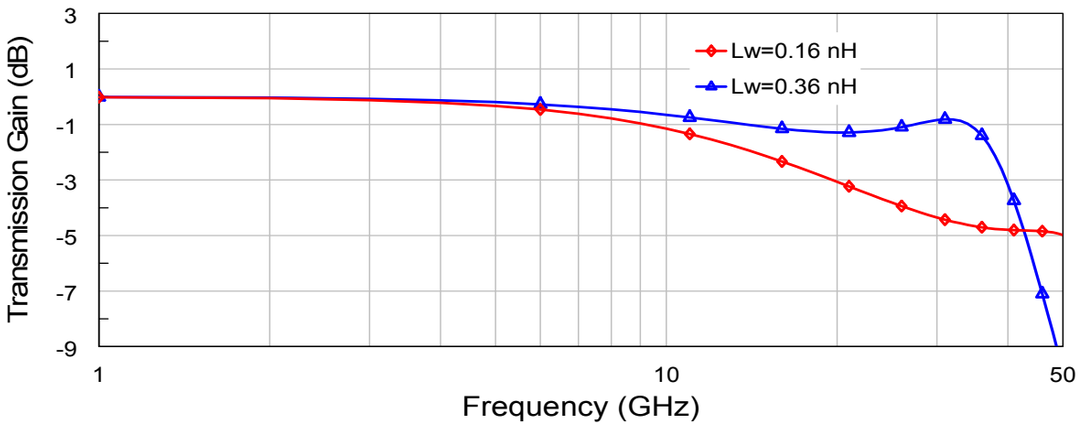

Fig. 9. The photodiode packaging effect simulation

3.3 Experimental verification

Based on the above simulation results some p-i-n photodiode samples were produced and mounted into the microwave microstrip test fixture. The typical time response of the photodetector sample measured by the two-section mode-locked laser and high-speed sampling oscilloscope is shown in the Figure 10. The pulse duration from the Figure is near 10 ps, so the accuracy of the above simulation results is verified.

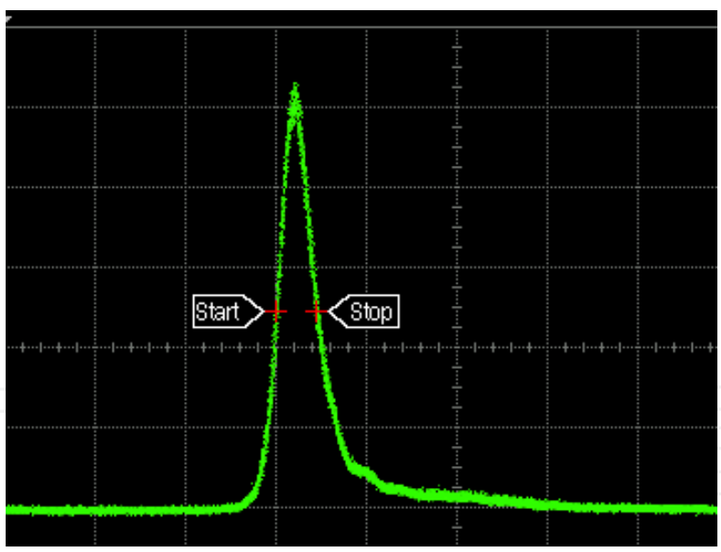

Fig. 10. Experimental photodiode impulse response (horizontal scale 25 ps/div.)

Thus, the methodology of the end-to-end computer-aided design for a p-i-n photodiode with microwave bandwidth is addressed. First, using the technology CAD tool a designer can define and optimize the dependence of the major photodiode structure parameters (absorption layer doping density and thickness, photosensitive window diameter, so on) on small-signal bandwidth and get the data for the following calculations. Then the electronic MW-CAD simulation based on the photodiode electrical equivalent circuits is performed that allow to take into account various effects in real receiver module with microwave

bandwidth: LC package parasitics, matching networks, front-end amplifier and so on. To confirm the actuality and accuracy of the proposed methodology the specific p-i-n photodiode with bandwidth of near 30 GHz was simulated. The simulation results were experimentally verified with fine accuracy.

4. Solitary MW-ECAD simulation

The main concept of this approach can be formulated as follows: a designer of analog receiving modules usually does not know a lot about the PD heterostructure's specific parameters, usually has not an access to a specific cost-expensive TCAD tool but he has facilities suitable for measuring transmittance and reflectance (or S-parameters) of the photodiode chip under test in the optical system's modulation band. Then equipped with experimental results, and equivalent circuit interpretation as well as AWRDE or another MW-ECAD tool facilities he builds up a non-linear "optoelectronic" equivalent circuit and if necessary some linear or nonlinear electronic circuits behind it.

4.1 P-i-n photodiode nonlinear model

Figure 11 represents cascaded equivalent circuit of PD that does it quite effective for simulation by means of a highly-developed MW-ECAD tool. There are two sub-circuits inside it: linear (right) and nonlinear (left). The linear sub-circuit simulating the frequency distortions due to parasitic elements impact agrees with small-signal PD model of Fig. 8. The nonlinear sub-circuit includes a diode D1 and a capacitance of p-n junction that is changed in according with applied reverse voltage (element PNCAP). To supply the nonlinear elements a DC source V2 is introduced. Inductance L1 is assigned for DC/AC isolation; resistance R2 models PD's DC termination. Non-ideality, phase shift, and delay of the optical-to-electrical conversion process are modeled by voltage-controlled current source U1.

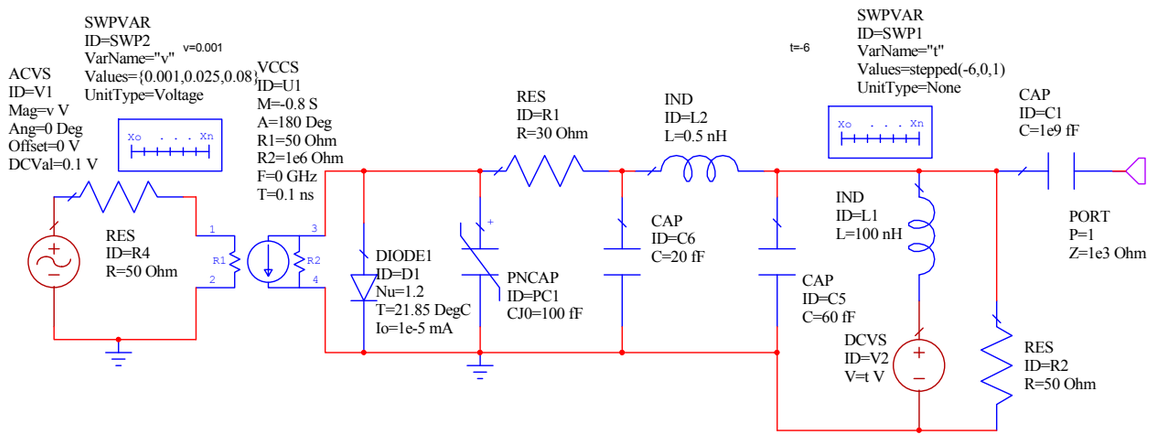

Fig. 11. MW-ECAD nonlinear p-i-n photodiode model based on electrical equivalent circuit

For the simulation an equivalent electrical AC source V1 is placed at the circuit input. A frequency of this source is tuned through the microwave-band modulation bandwidth, and its amplitude is in exact numerical agreement with a power of intensity-modulated optical signal. As it follows from Figure 11 for the given model experiment the next values are assumed: an equivalent power of optical carrier is 100 mW (DC voltage 0.1 V), equivalent

modulated optical power is changed in the range of 10-100 mW (0.01-0.1 V) that meets the optical modulation rate between 10 and 100 percentage. A reasonableness of the optoelectronic circuit's simulation by ECAD tool is founded on the proposed method of equivalent voltage which uses identical linear dependences of a current vs. voltage in an electrical circuit and a photocurrent vs. optical power in an optoelectronic circuit of a photoreceiver.

Thus, the next linear or nonlinear effects are taken into account in the given model: (i) nonlinearity of depletion layer capacity; (ii) frequency distortions due to parasitic elements of the PD package and receiver circuitry; (iii) reflections from photosensitive window; (iv) dark current and its dependence of temperature and bias voltage; (v) DC photocurrent generation due to optical carrier impact; (vi) deviation of the optical signal modulation rate; (vii) electric field screening due to series resistance.

4.2 Simulation results and discussion

At the first step, to calibrate the model the device-under-test small-signal frequency characteristics are simulated. As the result, 3-dB bandwidth is limited in the range of 20-30 GHz depending on reverse bias voltage and agreed well with the Figure 9 at the bias of 10 V. Then, the above-described three nonlinear distortion parameters depending on equivalent input optical power and reverse bias (Ub) are simulated through one-button operations. Figure 12 shows an example of equivalent AM-to-PM distortion characteristics at the fundamental frequency 15 GHz.

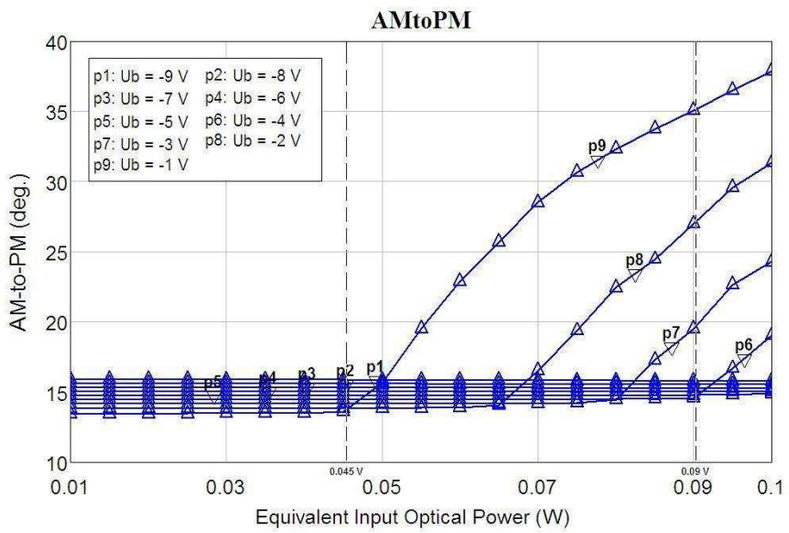

Fig. 12. Photodiode power to phase conversion characteristics

Also Figure 13 depicts an example of OIP2 characteristics for the input tones of 5 GHz and 6 GHz, and distortion tone of 11 GHz. At last Figure 14 shows an example of OIP3 characteristics for the input tones of 5 GHz and 5.1 GHz, and distortion tone of 4.9 GHz.

A combined outcome from Figures 12-14 follows that large-signal conversion features of a p-i-n photodetector are notably degraded as far as negative reverse DC bias is increased that is quite coincided with the experimental data of Table 1. In particular, Figure 12 depicts that

the PPC linearity threshold is twofold as the PD bias is decreased from -1 to -4 V. Also from Figure 13 one can see that second-order output intercept points are almost constant vs. optical power and their numerical deviations vs. bias are near 26 dB (from 47 dBm at -8 V to 21 dBm at -1 V). In spite of this, shown in Figure 14 third-order output intercept points begin to degrade with optical power at the bias more than -4 V, and their numerical deviations vs. bias are near 17 dB (from 44 dBm at -8 V to 27 dBm at -1 V). Note that the results of power-to-phase conversion simulation are comparable in principle with recent experimental data (Tailor et al., 2011), also the results of OIP2 and OIP3 simulation are closed to recent experimental data of Table 1.

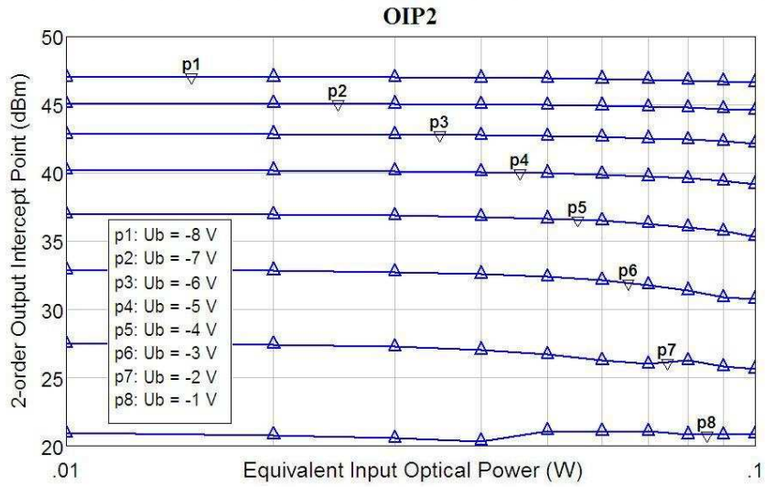

Fig. 13. Output second-order intercept point characteristics

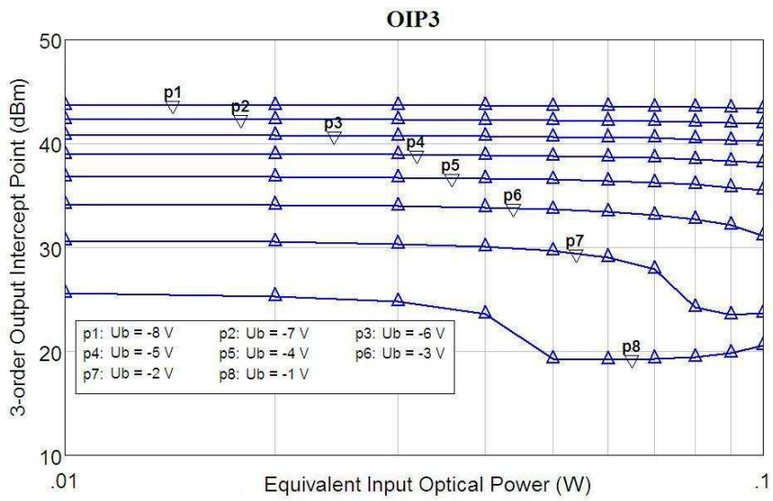

Fig. 14. Output third-order intercept point characteristics

Generally, based on our model experiments we are able to state that simple in design and producing cost-effective top-illuminated photodetector has been inspected holds somewhat (3-5 dB) lower linearity as compared to a special high-linear charge-compensated modified uni-traveling carrier photodiode (see Table 1). But the latter has at the same time

significantly higher bandwidth running up to THz band (Nagatsuma et al., 2007). Nevertheless the researched type of photodetector thanks to inherent cost-effectiveness also has a potential for RoF systems and microwave photonics applications with moderate frequency and power requirements.

For example, the typical values of the allowable AM-to-PM distortion and OIP3 for middle-power reasonable-noise microwave amplifiers are not more than 10^{o} as well near 30-35 dBm correspondently. Following it we are able to conclude: (i) even a standard p-i-n photodetector is more linear circuit element than pre-amplifier and can be used without it in the most photoreceiving schemes of microwave photonics devices and RoF system's photonic antennas; (ii) to secure a comparable p-i-n photodetector linearity the reverse bias voltage must be less than -4 V at optical power up to 100 mW.

5. Comparison of OE-CAD and MW-ECAD photodiode simulations

As we communicated in Introduction, the available optoelectronic CAD tools are unpractical for designing nonlinear device operating in microwave band. That's why it is in essential importance to state the numerical value of error while simulating for instance noise features of a photodetector in microwave band using MW-ECAD and OE-CAD software. Our direct comparison was fulfilled by AWRDE and advanced OE-CAD tool VPItransmission Maker™ version 8.6.

In the case of VPI software a library p-i-n photodiode model considering thermal and shot noise sources and dark current of 0.15 nA was selected. On the other hand, for photodiode MW-ECAD simulation the equivalent circuit model of Fig. 11 was used. For the both simulating experiments a broadband Gaussian-distributed white noise generator model with identical power levels was employed as a source. Varying its levels output noise power was measured in the band from 1 GHz to 50 GHz by the noise analyser model in the bandwidth of 1 Hz. Figure 15 depicts the simulation results.

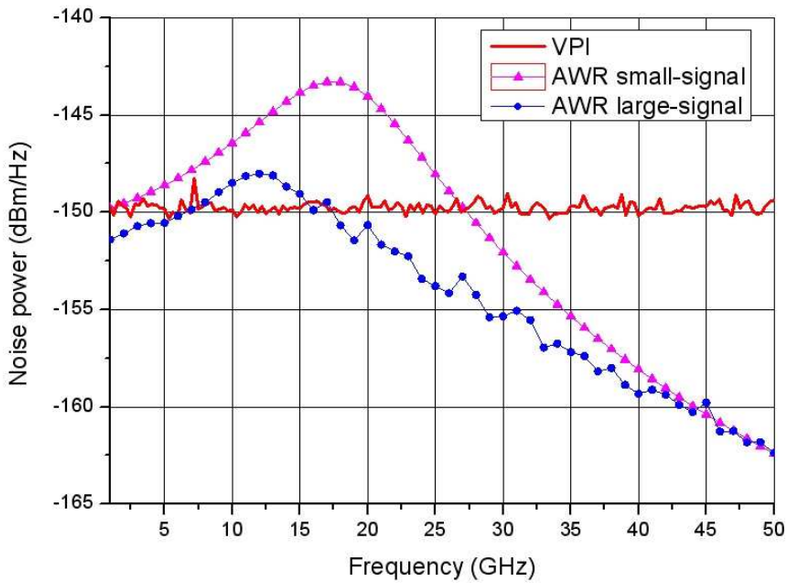

Fig. 15. OE-CAD tool vs. MW-ECAD tool simulation

As shown from Figure, simulated by VPI (solid curve) spectral density of average output noise power represents frequency and noise source power independent horizontal line that is unrealistic. On the other hand, simulated by AWRDE results follow the real frequency characteristic of the photodiode under test and differ subject to small-signal (triangles) or large-signal (circles) power regime of the noise source. The numerical value of error is up to 10 dB.

6. Conclusion

This chapter presented a multiscale approach to the combined TCAD&ECAD and solitary MW-ECAD simulations for designing a microwave-band p-i-n photodetector as a basic component of the receiving modules for radio-over-fiber systems and microwave photonics devices. Within the limits of the first approach, primarily, using a TCAD tool a designer can define and optimize the dependence of the major photodiode structure parameters on small-signal bandwidth. Then an electronic MW-CAD simulation based on the photodiode electrical equivalent circuits is performed that allow to take into account various effects in real receiver module with microwave bandwidth. To confirm the actuality and accuracy of the proposed methodology the specific p-i-n photodiode with bandwidth of near 30 GHz was simulated. The main concept of the second approach can be formulated as follows: a designer of analog receiving modules usually does not know a lot about the PD heterostructure's specific parameters, usually has not an access to a specific cost-expensive TCAD tool but he has facilities suitable for measuring transmittance and reflectance of the photodiode chip under test in the optical system's modulation band. Then equipped with experimental results, and equivalent circuit interpretation as well as AWRDE or another MW-ECAD tool facilities he builds up a non-linear "optoelectronic" equivalent circuit and if necessary some linear or nonlinear electronic circuits behind it. Following the simulation results we have concluded: (i) even a standard p-i-n photodetector is more linear circuit element than pre-amplifier and can be used without it in the most photoreceiving schemes of microwave photonics devices and RoF system's photonic antennas; (ii) to secure a comparable p-i-n photodetector linearity the reverse bias voltage must be less than -4 V at optical power up to 100 mW.

The modeling results are validated by the experimental data for TCAD&ECAD similation and by close agreement with the known measured data for MW-ECAD large-signal simulation.

7. Acknowledgment

This work was supported by the Russian Ministry of Education and Science program "Progress of scientific potential of the higher school (2009-2011)". Author wishes to thank Dr. E. Portnoi from Ioffe Physico-Technical Institute RAS for the mode-locked laser's photodiode measurement.

8. References

Agethen, M., et.al. (2002). InGaAs pin Detectors for Frequencies above 100 GHz, *IEEE Indium Phosphide and Relative Materials Conference, IPRM'2002*, A8-2, pp. 673-676

Beling, A., Pan, H., Chen, H. & Campbell, J.C. (2008). Measurement and modeling of high-linearity modified uni-traveling carrier photodiode. *IEEE Photonics Technology Letters*, Vol.20, No.14, (July 2008), pp. 1219-1221, ISSN 1041-1135

Beling, A. & Campbell, J.C. (2009). InP-Based High Speed Photodetectors, *IEEE Journal of Lightwave Technology*, Vol. 27, No 3, (February 2009), pp. 343-355

Belkin, M.E., Dzichkovski, N.A. & Indrishenok.V.I. (2008). Super high-speed p-i-n-photodiode heterostructures computer simulation. *Journal of Nano and Microsystem Techniques*, No 10 (99), (October 2008) pp. 23 – 28, (in Russian)

Belkin, M.E. & Dzichkovski, N.A. (2009). Research of microwave-bandwidth p-i-n photodetectors, *Proceedings of EUROCON* 2009, p.193-196, St. Peterburg, Russia, May 2009

Blakey, P.A. (2008). Technology CAD. In: *RF and Microwave Circuits, Measurements, and Modeling*, M. Golio, J. Golio, (Ed.), Boca Raton, 34-1 – 34-11, ISBN 13-978-0-8493-7218-6, London

Bowers , J. E. & Burrus C.A. Ultrawide-Band Long-Wavelength p-i-n Photodetectors, *IEEE Journal of Lightwave Technology*, vol. 5, No 10,(October 1987), pp. 1339-1350

Capasso, F., et. al. (1985). Photodetectors, In: *Lightwave Communications Technology,* Vol. 22, Part D, W.T. Tsang, (Volume Ed.), Academic Press Inc.

Draa, M.N., et al. (2008). Frequency behaviors of third order intercept point for a waveguide photodiode using three laser two-tone setup. *Proceedings of 21st Annual Meeting of the IEEE Lasers and Electro-Optics Society. LEOS 2008,* pp. 284-285, Acapulco, Mexico, November 9-13, 2008

Godinez, M.E., et al. (2008). RF Characterization of Zero-Biased Photodiodes. *IEEE Journal of Lightwave Technology*, Vol. 26, No 24, (December 2008), pp. 3829-3834

Gustavsson, M., Hedekvist, P.O. & Andrekson, P.A. (2005). Uni-Travelling-Carrier Photodiode Performance with X-band Modulation at High Optical Power. *IEEE Microwave and Wireless Components Letters*, v.15, No.5, (May 2005), pp. 297-299, ISSN 1531-1309

Itakura, S., et al. (2010). High-Current Backside-Illuminated Photodiode Array Module for Optical Analog Links. *IEEE Journal of Lightwave Technology*, Vol. 28, No 6, (March 2010), pp. 965-971, ISSN 0733-8724

Jiang, H. et al. (2000). The Frequency Behavior of the Third-Order Intercept Point in a Waveguide Photodiode. *IEEE Photonic Technology Letters*, Vol.12, No.5, (May 2000), pp. 540-542

Joshi, A., Datta, S. & Becker, D. (2008). GRIN Lens Coupled Top-Illuminated Highly Linear InGaAs Photodiodes. *Photonics Technology Letters*, Vol.20, No.17, (September 2008), pp. 1500-1502, ISSN 1041-1135

Joshi, A. & Datta, S. (2009). Highly Linear, High Power Handling Photodiode for RF Photonic Links, *Proceedings of ECOC 2009*, p. 9.2.4, Vienna, Austria , 20-24 September 2009

Kenington, P.B. (2000). *High-Linearity RF Amplifier Design*. Artech House, ISBN 1-58053-143-1, Norwood, MA

Kielmeyer, R. (2008). Computer Aided Design (CAD) of Microwave Circuitry. In: *RF and Microwave Circuits, Measurements, and Modeling,* M. Golio, J. Golio,, (Ed.), Boca Raton, 31-1 – 31-8, ISBN 13-978-0-8493-7218-6, London

Li, Z., et al. (2010). High-Saturation-Current Modified Uni-Traveling-Carrier Photodiode With Cliff Layer. *IEEE Journal of Quantum Elecronics,* Vol.46, No.5, (May 2010),pp. 626-632, ISSN 0018-9197

Liao, T.S. et al. (2003). Investigation of the High Power Integrated Uni-Traveling Carrier and Waveguide Integrated Photodiode, *IEEE 2003 MTT-S International Microwave Symposium Digest*, pp. 155-158, vol.1, Philadelphia, PA, 8-13 June, 2003

Lowery, A.J. (1997). Computer-aided photonics design. *IEEE Spectrum,* Vol. 34, No 4 (April 1997), pp. 26-31, ISSN: 0018-9235

Minixhofer, R. TCAD as an integral part of the semiconductor manufacturing environment. (2006), *Proceedings of International Conference on Simulation of Semiconductor Processes and Devices, SISPAD*, pp. 9 – 16. Monterey, California, September 6-8, 2006

Nagatsuma, T., Ito, H. & Ishibashi, T. (2007). Photonic THz Sources Using Uni-Traveling-Carrier Photodiode Technologies. *Proceedings of LEOS 2007, International Topical Meeting of Laser and Electro-Optic Society,* pp. 792-793.

Pedro, J. C. & Carvalho, N. B. (2003). *Intermodulation Distortion in Microwave and Wireless Circuits*, Artech House, ISBN 1580533566, Boston, London

Ramaswamy, A. et al. (2009). Experimental analysis of two measurement techniques to characterize photodiode linearity. *Proceedings of MWP '09, International Topical Meeting on Microwave Photonics*, pp. 1-4, ISBN 978-1-4244-4788-6. Valencia, Spain, October 14-16, 2009

Sauer, M., Kobyakov, A. & George, J. (2007). Radio over Fiber for Picocellular Network Architectures, *IEEE Journal of Lightwave Technology*, vol. 25, no. 11, (November 2007), pp. 3301-3320

Taylor, J.A., et al. (2011). Characterization of Power-to-Phase Conversion in High-Speed P-I-N Photodiodes. *IEEE Photonics Journal*, Vol. 3, No.1, (February 2011), pp. 140 – 151, ISSN 1943-0655

Tulchinsky, D.A. et al. (2008). High Current Photodetectors as Efficient, Linear and High-Power RF Ouput Stages. *IEEE Journal of Lightwave Technology,* Vol. 26, No.4, (February 2008), pp. 408–416

Wey, Y.-G. et al. (1995). 110-GHz GaInAs/InP Double Heterostructure p-i-n Photodetectors, *IEEE Journal of Lightwave Technology*, vol. 13, No 7,(July 1995), pp. 1490-1499

Williams, K. J., Esman, R. D. & Dagenais, M. (1996). Nonlinearities in p-i-n Microwave Photodetectors., *IEEE Journal of Lightwave Technology*, vol. 14, No 1,(January 1996), pp. 84-96

Yao, J.P. (2009). Microwave Photonics, *IEEE Journal of Lightwave Technology*, vol. 27, No 3, (February 2009), pp. 314-335

Yao, X.S. (2002). Opto-electronic Oscillators, In: *RF Photonic Technology in Optical Fiber Links,* W. S. Chang(Ed.), 255-292, Cambridge University Press, Cambridge, UK

Yu, P. K. L. & Wu, M. C. (2002). Photodiodes for high performance analog links, In: *RF photonic technology in optical fiber links*, W. S. Chang, (Ed), 231-254, Cambridge university press, Cambridge, UK

Zakhleniuk, N.A. (2007). Theory and Modelling of High-Field Carrier Transport in High-Speed Photodetectors. *Proceedings of NUSOD'07 Numerical Simulation of Optoelectronic Devices*, pp. 77-78, ISBN 978-1-4244-1431-4, Newark, DE, September 24-28, 2007

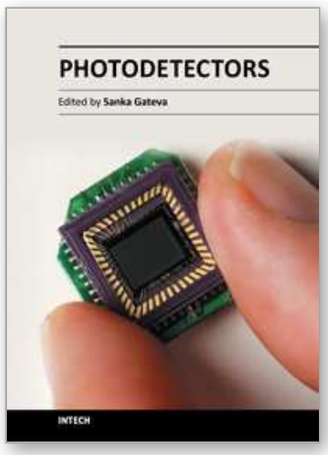

Photodetectors

Edited by Dr. Sanka Gateva

ISBN 978-953-51-0358-5
Hard cover, 460 pages
Publisher InTech
Published online 23, March, 2012
Published in print edition March, 2012

In this book some recent advances in development of photodetectors and photodetection systems for specific applications are included. In the first section of the book nine different types of photodetectors and their characteristics are presented. Next, some theoretical aspects and simulations are discussed. The last eight chapters are devoted to the development of photodetection systems for imaging, particle size analysis, transfers of time, measurement of vibrations, magnetic field, polarization of light, and particle energy. The book is addressed to students, engineers, and researchers working in the field of photonics and advanced technologies.

How to reference

In order to correctly reference this scholarly work, feel free to copy and paste the following:

Mikhail E. Belkin (2012). Multiscale Computer Aided Design of Microwave-Band P-I-N Photodetectors, Photodetectors, Dr. Sanka Gateva (Ed.), ISBN: 978-953-51-0358-5, InTech, Available from: http://www.intechopen.com/books/photodetectors/multiscale-computer-aided-design-of-microwave-band-p-i-n-photodetectors

INTECH
open science | open minds

InTech Europe
University Campus STeP Ri
Slavka Krautzeka 83/A
51000 Rijeka, Croatia
Phone: +385 (51) 770 447
Fax: +385 (51) 686 166
www.intechopen.com

InTech China
Unit 405, Office Block, Hotel Equatorial Shanghai
No.65, Yan An Road (West), Shanghai, 200040, China
中国上海市延安西路65号上海国际贵都大饭店办公楼405单元
Phone: +86-21-62489820
Fax: +86-21-62489821

IntechOpen